

Transient Interaction Between Reduction and Slagging Reactions of Wustite in Simulated Cohesive Zone of Blast Furnace



KAIHUI MA, JIAN XU , JUNYI DENG, DONGDONG WANG, YANG XU, ZHEHAN LIAO, CHENGFENG SUN, SHENGFU ZHANG, and LIANGYING WEN

The blast furnace cohesive zone plays an important role in the gas flow distribution and heat-transfer efficiency. Previous work mainly employed temperature-based indices to evaluate and predict the shape and thickness of the cohesive zone, whereas the internal reactions and related effects on the softening and melting properties of a complex burden are ignored. In this study, an innovative index, namely, shrinkage rate (SR), is first proposed to directly estimate the shrinkage behavior of wustite (FeO)-packed bed inside a simulated cohesive zone. The index is applied as the temperature increases to elucidate the transient interaction between reduction and slagging reactions. Results show that the thermally induced slagging reaction causes the packed bed to shrink at lower temperature, and the SR doubles when compounds with low melting temperature are generated by adding a reasonable concentration of CaO or SiO₂. The reduction reaction becomes the driving force during the shrinkage of the packed bed between 1173 K and 1273 K when CO is introduced in the mixture gas. Then, the dominating factors for further shrinkage include slagging, reduction, or both factors. These factors vary with respect to the added compounds or temperature.

<https://doi.org/10.1007/s11663-018-1307-7>

© The Minerals, Metals & Materials Society and ASM International 2018

I. INTRODUCTION

THE blast furnace cohesive zone serves as a transition region between the upper lump zone and lower dripping zone. This zone directly determines the secondary distribution of the gas flow and the heat transfer inside a high-temperature region.^[1] Thus, understanding the structure and the formation mechanism of the cohesive zone is highly important for the smooth operation and low carbon emission of a blast furnace.

The position and thickness of the cohesive zone is principally dependent on the softening and melting properties of its iron-bearing burden.^[2,3] Sinter, pellet, lump ore, and other raw materials have been employed to investigate the softening and melting behavior,^[4-8]

and various indices have been proposed to evaluate the effects of the added compounds on the formation of the cohesive zone.^[9-12] For example, Al₂O₃ was found to have priority over MgO to enter into a slag, and the latter mainly existed in the FeO-MgO solid solution.^[13] Thus, the softening temperature decreased, and the bed permeability deteriorated.^[4] By contrast, further increase in MgO concentration increased the softening temperature and the liquidus temperature of the slag.^[5] The general increase in the softening and melting interval not only increased the thickness of the cohesive zone but also moved its position downward. However, several works did not show that MgO greatly affected the softening properties of an iron-bearing burden.^[6,7] The softening, melting, and permeability of CaO-FeO-SiO₂ ternary mixture were also investigated.^[8]

The gaseous reduction of iron oxides has been studied based on thermodynamic and kinetics.^[9-14] However, most experiments have been performed below 1400 K.^[15-17] Wang *et al.* found that the replacement of N₂ by CO significantly increased the reduction rate at 1673 K.^[18] Thus, the gaseous reduction of iron oxide by CO in the blast furnace cohesive zone could not be neglected. Moreover, Inoue *et al.* found that the wustite (FeO) reduction rate constant increased when 0.5 pct of CaO in mass fraction was added.^[19] FeO doped with SiO₂ was also found to promote the reduction rate at

KAIHUI MA, JUNYI DENG, DONGDONG WANG, YANG XU, ZHEHAN LIAO, and CHENGFENG SUN are with the College of Materials Science and Engineering, Chongqing University, Chongqing 400044, China. JIAN XU, SHENGFU ZHANG, and LIANGYING WEN are with the College of Materials Science and Engineering, Chongqing University and also with the Chongqing Key Laboratory of Vanadium-Titanium Metallurgy and Advanced Materials, Chongqing University, Chongqing 400044, China. Contact e-mail: jxu@cqu.edu.cn

Manuscript submitted October 17, 2017.

Article published online June 12, 2018.

high temperature. This phenomenon was due to the larger pores and the less-dense metal, but the reduction process was retarded when the temperature was below 1000 K.^[20,21] Hayashi *et al.* found that FeO reduction was extremely suppressed by Al₂O₃ or SiO₂ because of the formation of dense iron, while the simultaneous dissolution of Al₂O₃ and SiO₂ accelerated FeO reduction.^[22]

Hence, although slagging and reduction reactions under simulated blast furnace cohesive zone conditions have been widely studied, several viewpoints are worthy of further exploration. For example, when an iron-bearing burden moves close to the cohesive zone of a blast furnace, the iron oxide is almost reduced to FeO by indirect reduction. At the same time, the gangue, which consists of CaO, SiO₂, MgO, and Al₂O₃, is likely to form a slag phase with FeO as the temperature increases. FeO can be further reduced to metallic iron or can form a slag with the gangue (Figure 1). Thus, exploring the interaction between reduction and slagging reactions in the cohesive zone formation is intriguing. Moreover, although the use of transient temperature-based indices to evaluate the structure of the cohesive zone have been recommended based on previous softening and melting experiments, the actual temperature distribution inside a

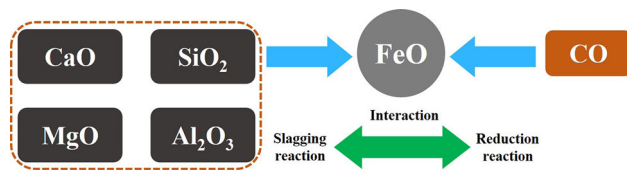


Fig. 1—Interaction between the reduction and slagging reactions of FeO.

blast furnace is very difficult to measure. Thus, the thickness of the cohesive zone cannot be predicted directly.

In the present study, a new parameter, namely the shrinkage rate (SR), is defined and applied to quantitatively determine the changes in the thickness of the cohesive zone. Then, the transient interactions between the reduction and slagging reactions with respect to temperature are investigated by simulating the cohesive zone conditions. These interactions are further discussed based on the binary slag composition.

II. EXPERIMENTAL PREPARATION, APPARATUS, AND CONDITIONS

A. Sample Preparation

The preparation of FeO and binary mixture samples are schematically demonstrated in Figure 2. For the FeO samples, the ferrous oxalate powders (FeC₂O₄·2H₂O, 99.9 pct, < 200 μm) are first pressed into a cake under the load of 10 kPa, and 5 g of water is added as the binder. The cylinder-shaped cake is 30 mm high with cross-sectional diameter of 40 mm (Figure 3). The cakes are placed on a homemade support made of steel and loaded into the three-stage resistance furnace (Figure 4). The decomposition reaction is carried out at 1023 K for 1 hour and requires continuous introduction of N₂ (99.99 pct purity) as shield gas to protect the products, that is, FeO samples, from oxidation. The composition is measured by XRD (PANalytical B.V. D/max2500/PC Cu K_α) after the prepared samples are cooled to room temperature. The results show that the FeO samples are well prepared (Figure 5(a)). Then, the samples are broken into small ones in the size range of 6 to 8 mm for the subsequent softening–melting experiments (Figure 5(b)).

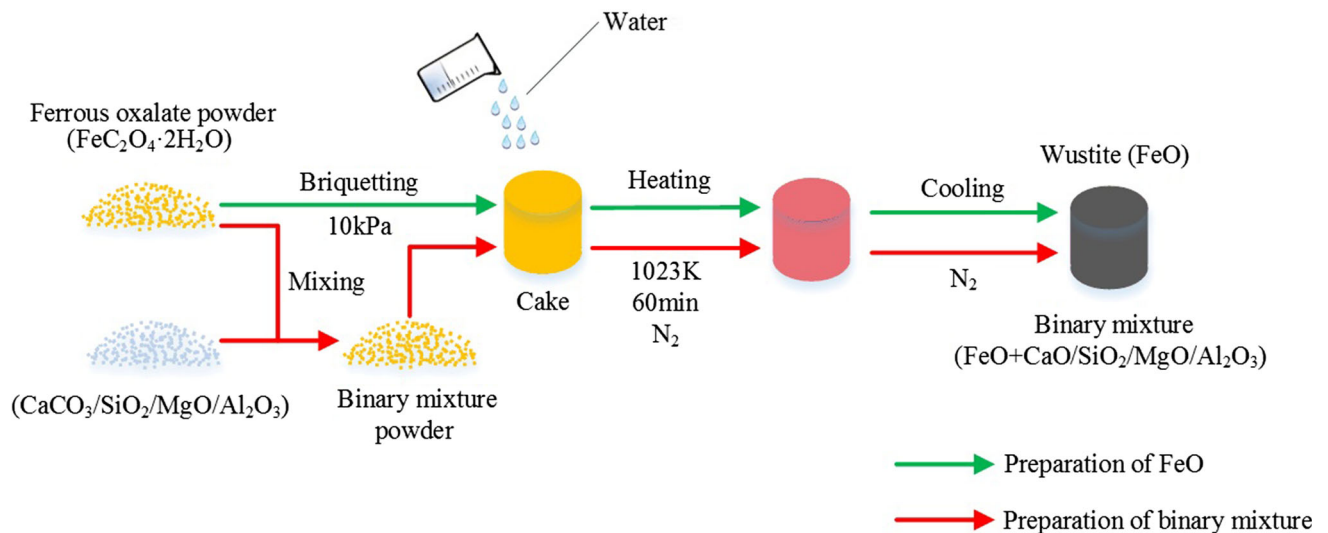


Fig. 2—The preparation of FeO and binary mixture samples.

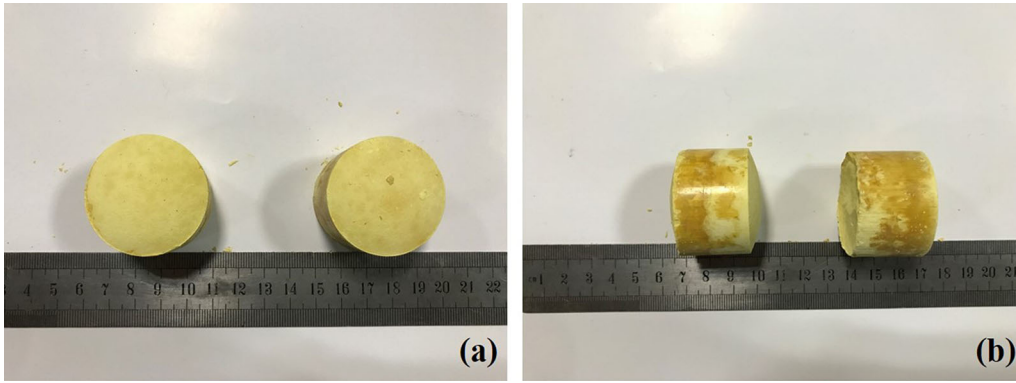


Fig. 3—Dimension of the cylinder-shaped cake (a) top view of cross section and (b) side view of height.

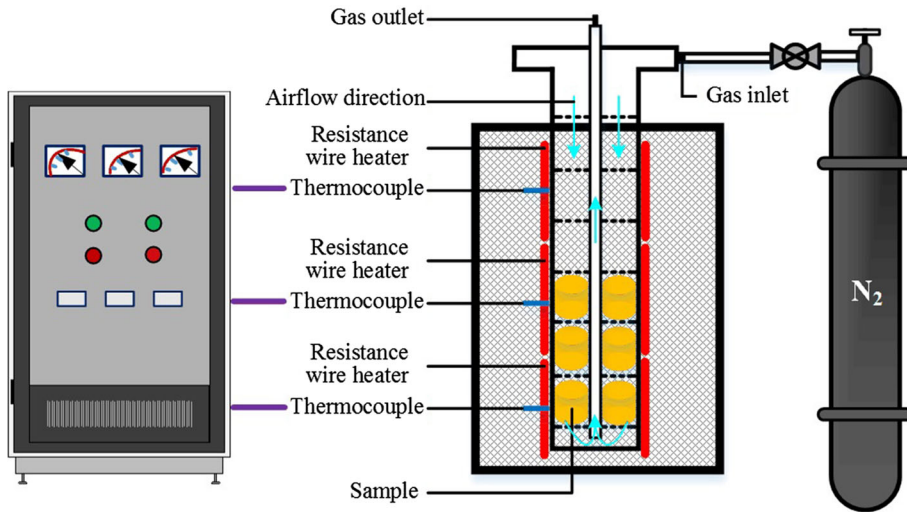


Fig. 4—Schematic diagram of the three-stage resistance furnace for the decomposition reaction.

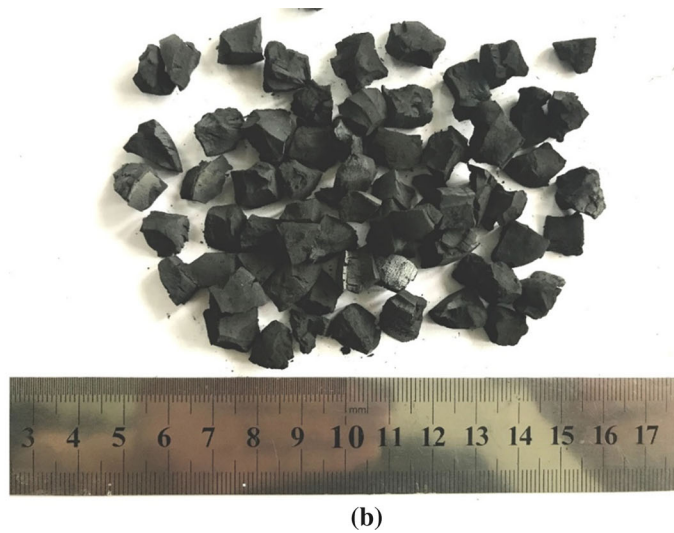
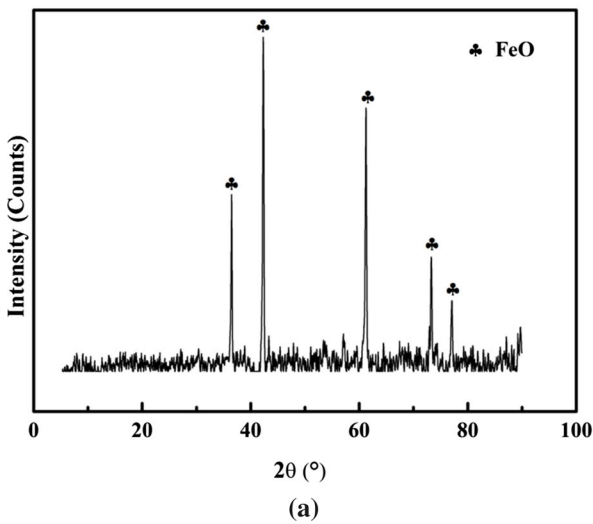


Fig. 5—Prepared FeO samples for the subsequent softening–melting experiment (a) the composition measured by XRD and (b) the appearance with size of 6 to 8 mm.

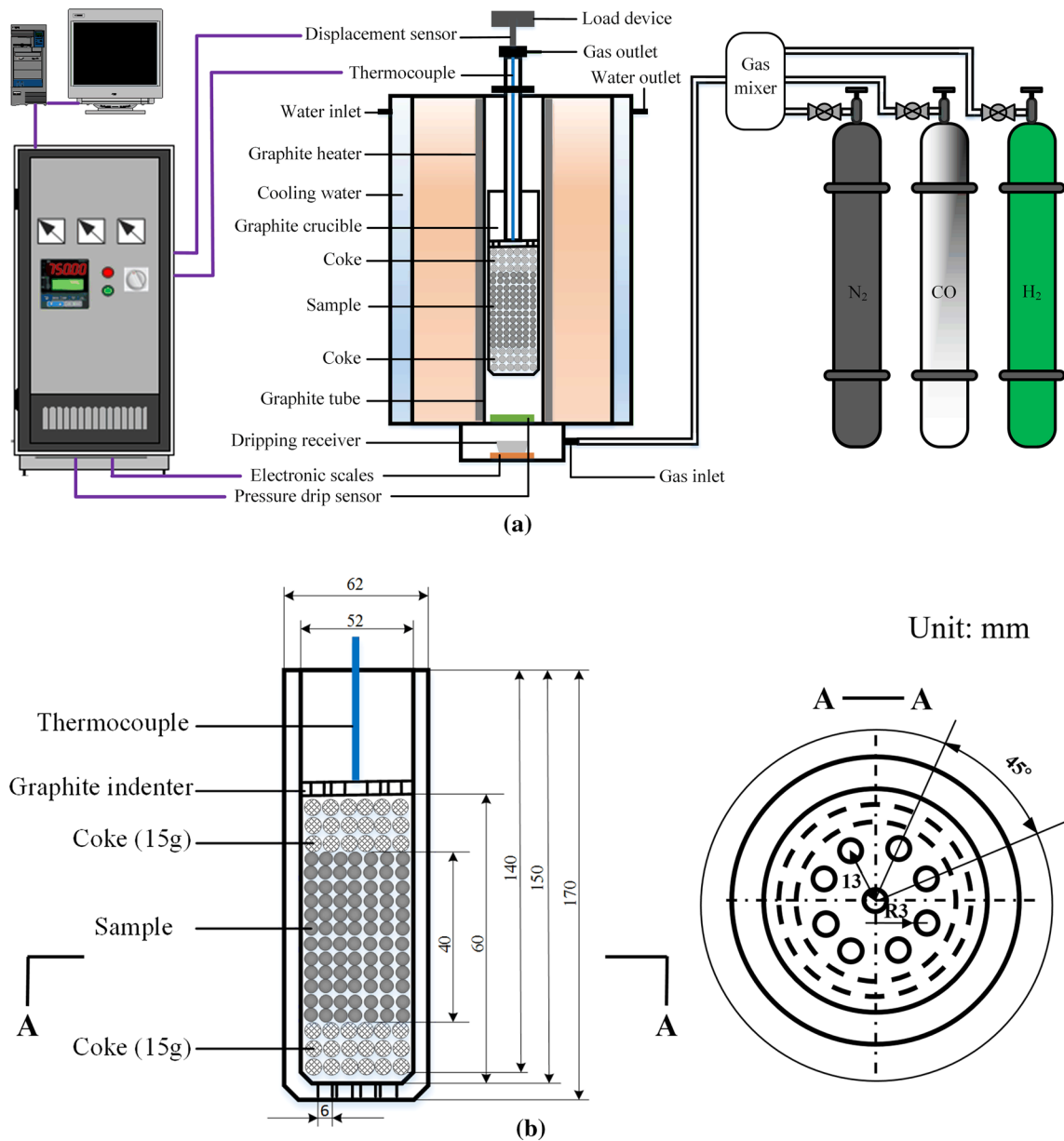


Fig. 6—Schematic diagram of the experimental apparatus for the softening–melting experiment (a) the main parts and (b) the detailed dimensions of the graphite crucible.

B. Experimental Apparatus and Conditions

The schematic diagram of the experimental apparatus for the softening–melting experiment is shown in Figure 6(a). The apparatus consists of four parts, namely, temperature controller, heating furnace, data collecting system, and gas supply and mixer system. The load device is installed on the top of the heating furnace to simulate the effective load applied by the burden packed bed above the simulated cohesive zone. A displacement sensor is used to record changes in the height of the packed bed during the experiment. Simultaneously, the mixture gas is introduced from the bottom into the graphite crucible and then discharged through the top gas outlet. The pressure drop is recorded by a

sensor installed at the bottom. In addition, a dripping receiver is used to measure the weight of the samples once dripped. The inner diameter of the graphite crucible is 52 mm and its total height is 150 mm (Figure 6(b)). Moreover, 9 holes (1 hole at the center and 8 holes in the periphery) with diameter of 6 mm are uniformly distributed at the bottom. A three-layer burden is placed in the crucible, and the upper and lower layers consist of 15 g of coke samples with size of 8 to 10 mm. The middle layer, with an initial height of 40 mm, consists of FeO samples with size of 6 to 8 mm. The average porosity of the three-layer packed bed is 31.4 pct. An S-type thermocouple is placed close to the burden surface to record the temperature every 2 seconds.

The experimental conditions are explained in Figure 7. The heating rate is 10 K/min below 1173 K under N₂ atmosphere, and the gas flow rate is 5 L/min. Then, the heating rate shifts to 5 K/min, and the reducing gas consists of CO:N₂ = 40:60 in the mole ratio when the gas flow rate is 10 L/min. A constant load of 0.1 MPa is applied above the three-layer burden packed bed. The experiment ends when no significant change is observed in the displacement. Finally, the samples are cooled to room temperature under N₂ atmosphere with a flow rate of 5 L/min.

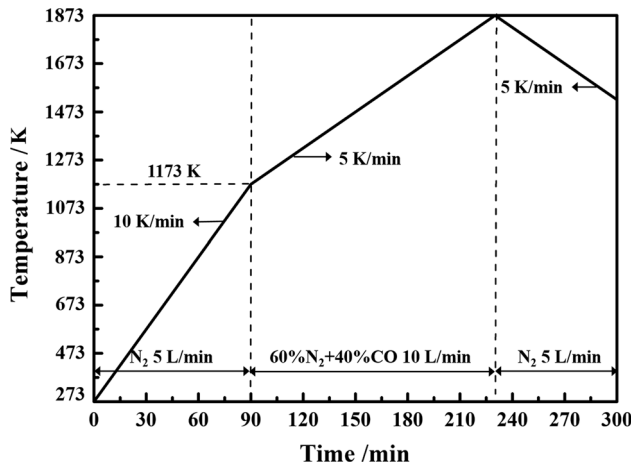


Fig. 7—Experimental conditions for the softening–melting experiment.

III. INTERACTION BETWEEN REDUCTION AND SLAGGING OF FeO (BASE CASE)

A. Experimental Schemes

In the base case study, two kinds of gas compositions, namely, 40 pct CO + 60 pct N₂ (FeO-CO scheme) and 100 pct N₂ (FeO-N₂ scheme) in the mole fraction, are introduced to study the interaction between reduction and slagging of FeO in the simulated cohesive zone.

B. Results and Discussion

1. Analysis of FeO-CO scheme

In a typical result of a softening–melting experiment,^[23–26] $T_{10 \text{ pct}}$ is the temperature when the samples shrink by 10 pct, indicating that the samples begin to soften. $T_{40 \text{ pct}}$ is the temperature when the samples shrink by 40 pct, indicating the end of the sample softening stage. T_m is the temperature when the pressure drop of the packed bed reaches 0.98 kPa, indicating that the generation of the initial slag. T_p is the temperature when the pressure drop reaches its peak value, during which the samples have basically melted. T_d represents the dripping temperature. $T_{40 \text{ pct}} - T_{10 \text{ pct}}$ is the softening temperature interval, while $T_d - T_m$ is the melting temperature interval.

For FeO-CO, the experiment runs twice, and the results are compared in Figure 8. FeO exhibits an initial and steep shrinkage between 973 K and 1173 K. As soon as CO is introduced, FeO begins to be reduced and further shrinks by 40 pct, and the pressure drop simultaneously peaks and then decreases to zero.

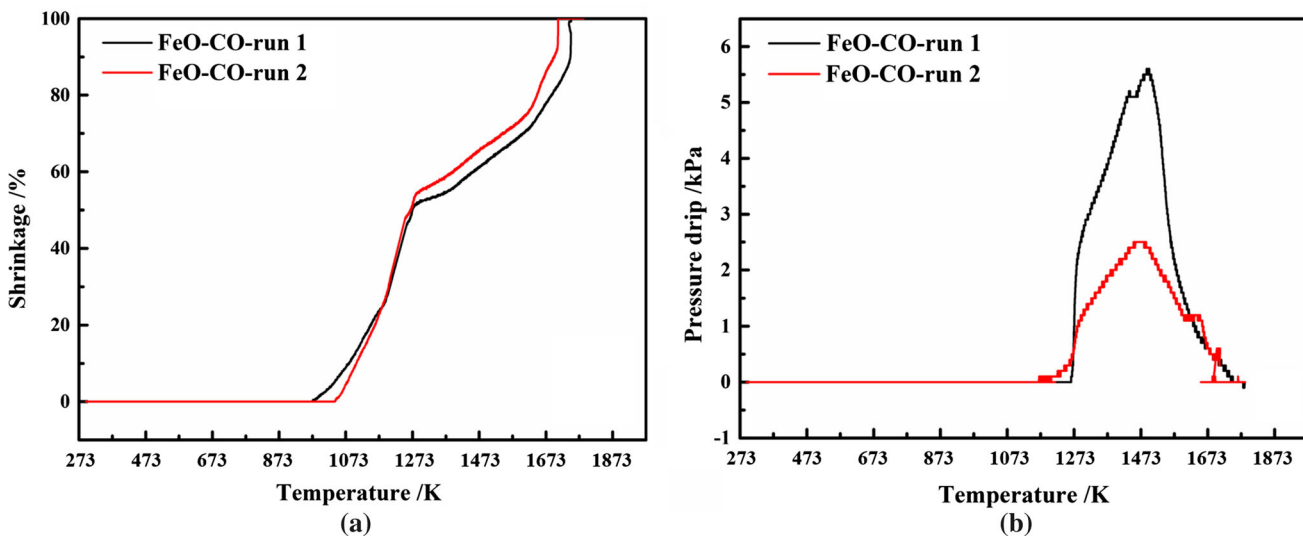


Fig. 8—The softening–melting experimental results of FeO-CO scheme (a) shrinkage vs temperature and (b) pressure drop vs temperature.

The softening–melting indices of the FeO–CO scheme are listed in Table I. The results show that the softening start temperature is between 1083 K and 1105 K, and the end temperature is between 1233 K

and 1241 K. Meanwhile, the melting start temperature is approximately 1278 K, and its end temperature is between 1709 K and 1783 K. In addition, the maximum pressure drop is between 2.5 and 5.6 kPa.

Table I. The Softening–Melting Indices of FeO–CO Scheme (Unit: K)

	Softening Start Temperature	Softening End Temperature	Softening Interval	Melting Start Temperature	Melting End Temperature	Melting Interval
FeO–CO run 1	1083	1241	159	1273	1783	509
FeO–CO run 2	1105	1233	128	1281	1709	428

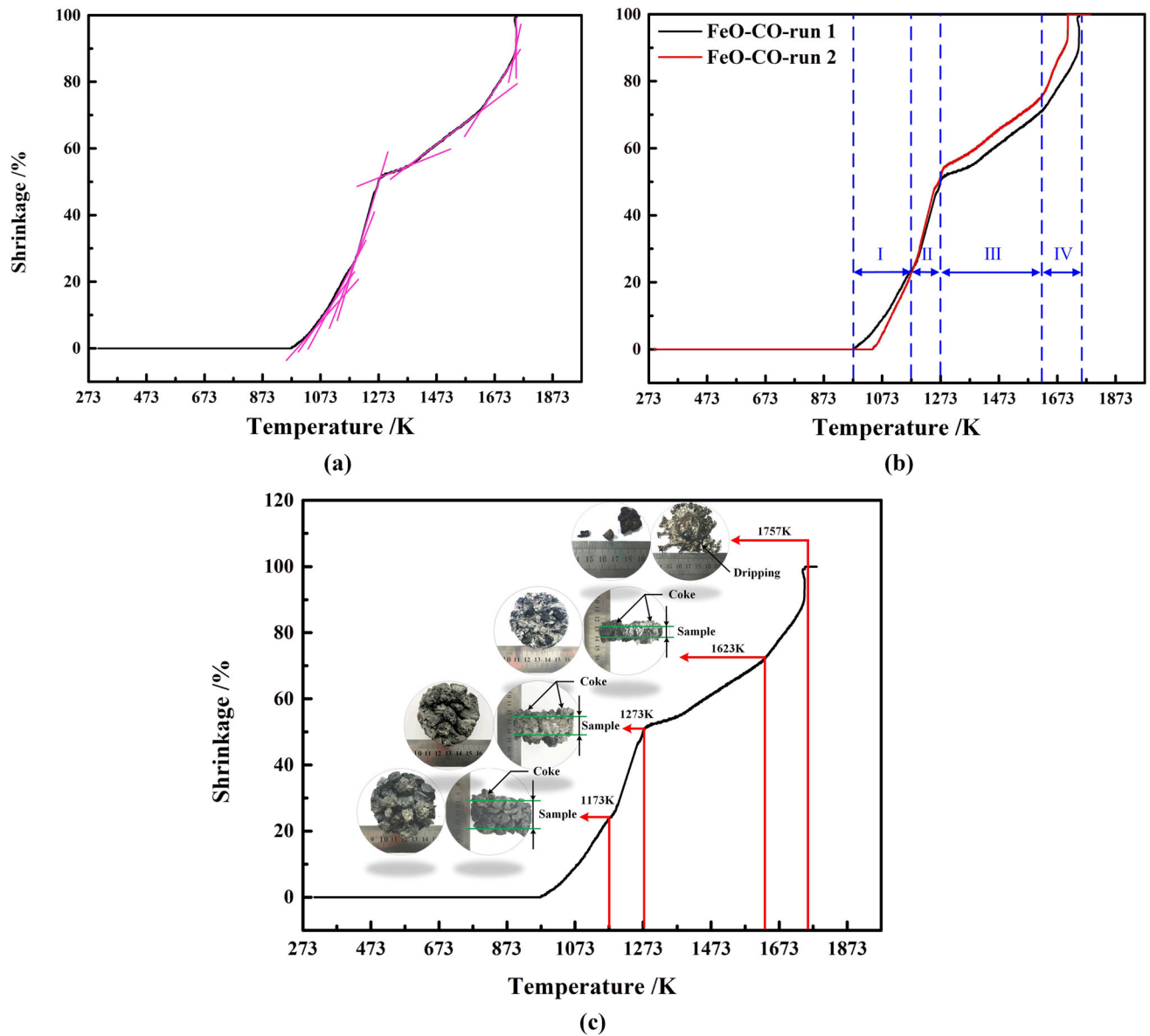


Fig. 9—The divided stages of the shrinkage curve with respect to the temperature in FeO–CO scheme (a) schematic diagram of the tangents to the curve at the different temperature, (b) the obtained four stages, and (c) the interrupted results at the boundary temperature between the adjacent stages.

Relatively remarkable difference is observed in the temperature-based indices between the two-run experimental results. The softening interval in FeO-CO run 1 case is 159 K, while that in run 2 case is 128 K. Thus, the latter is 20 pct smaller than the former. Complex factors, such as packed bed structure, particle size, and temperature control operation, lead to the poor repeatability of the temperature-based results. Moreover, the aim of the softening–melting experiment is to simulate the cohesive zone inside blast furnace, but previous indices mainly focused on the transient temperature, but the changes in thickness of the cohesive zone are neglected. Therefore, SR is proposed to reevaluate the shrinkage behavior of iron oxides under the simulated cohesive zone conditions.

The SR is defined by Eq. [1]. The initial height of the FeO sample packed bed is 40 mm (denoted by H_0) as explained in Section II–B, and the transient height (denoted by H_i) with respect to the increasing temperature is recorded. The corresponding dimensionless shrinkage is calculated as $(H_0 - H_i)/H_0$. The dimensionless shrinkage over the temperature is determined as the SR. Hence, the slope of the tangent to the curve (shrinkage vs temperature) represents the SR, and its unit is in percentage per Kelvin (pct/K).

$$SR = \Delta \frac{H_0 - H_i}{H_0} / \Delta T. \quad [1]$$

In addition, the measurement accuracy of the displacement sensor is 1 mm, and the initial packed bed height is 40 mm. This parameter has two significant figures. Meanwhile, the measurement accuracy of temperature is 1 K. Hence, this parameter will have three or even four significant figures when the temperature is above 973 K. Hence, the calculated SR has two significant figures.

The curve in Figure 8(a) is divided into several stages based on the experimental conditions and the slopes of tangents. When the temperature is lower than 1173 K, the heating rate is 10 K/min, and only N₂ is injected (Figure 7). Thus, the first stage is defined from the point when the packed bed begins to shrink up to the point when the temperature reaches 1173 K. Then, the experimental conditions are kept constant. The division of the curve is decided by comparing the calculated slopes of the tangents to the curve at the different temperatures (Figure 9(a)). The curve is divided into four stages and redrawn in Figure 9(b), in which, I, II, III, and IV,

represent the first, second, third, and fourth stages, respectively. The SR of each stage is calculated, and the results are compared in Table II.

In the first stage, only the increasing temperature causes FeO to deform and fill the pores in the initial packed bed, because no reducing gas is introduced. This phenomenon results in a steep shrinkage in the diagram. The photos of the samples are shown in Figure 9(c) when the experiment is interrupted at 1173 K. The thickness of the packed bed decreases from 40 mm to approximately 30 mm, and the average SR is 0.17 pct/K. Once the reducing gas CO is introduced in the second stage, the reduction from FeO to metallic iron speeds up the shrinking process, and the average SR doubles to 0.31 pct/K. The corresponding thickness further decreases to approximately 20 mm at 1273 K. By contrast, in the third stage, when the proportion of produced metallic iron in the packed bed increases, the enhancement on the shrinkage by the reduction process is greatly suppressed, and the average SR drops to as low as 0.067 pct/K. The metallic iron penetrates the coke layer below, and the thickness of the packed bed is 11 mm at 1623 K. In the final stage, when the temperature further increases, the remaining FeO begins to melt. When the temperature approaches 1757 K, the reduced metallic iron after carbonization gradually melts and drips. This phenomenon increases the average SR to 0.18 pct/K.

2. Comparison between FeO-CO and FeO-N₂ schemes

The shrinkages with respect to the temperature under CO-N₂ and sole N₂ are compared in Figure 10, and the corresponding SRs in the different stages are listed in Table II. For FeO-N₂, the curve is divided into three stages, and the boundary between the first and second stages is located at 1173 K, similar to that in FeO-CO. The boundary between the second and the third stages is located at 1573 K. The average SR in the first stage of FeO-N₂ scheme is 0.20 pct/K. Theoretically, this value should be identical to that in FeO-CO because of the same experimental conditions. Thus, the discrepancy is ascribed to the difference in the initial packed bed structure. Moreover, the shrinkage is principally affected by the slagging reaction because no reducing gas is injected. The second and third stages in the FeO-CO scheme are approximately merged into a new second stage. After the pores in the initial packed bed have been completely filled in the previous stage, the average SR decreases to 0.043 pct/K. When the

Table II. The SRs of Different Stages in FeO-CO and FeO-N₂ Schemes (Unit: pct/K)

Schemes	First Stage	Second Stage	Third Stage	Fourth Stage
FeO-CO-run 1	0.15	0.29	0.067	0.15
FeO-CO-run 2	0.18	0.33	0.066	0.20
Average value	0.17	0.31	0.067	0.18

Schemes	First Stage	Second Stage	Third Stage
FeO-N ₂ -run 1	0.21	0.044	0.35
FeO-N ₂ -run 2	0.19	0.041	0.47
Average value	0.20	0.043	0.41

temperature exceeds 1573 K, the following reactions or processes positively contribute to the bed shrinkage: the direct reduction participated by coke and FeO becomes increasingly important; the unreacted FeO demonstrates serious softening behaviors, because the temperature is close to the melting point; and the produced metallic iron begins to melt and drip after carbonization. Consequently, the combined effects increase the average SR up to 0.41 pct/K, which proves again that the reduced metallic iron resists the shrinkage of the packed bed before 1623 K.

The interaction between the reduction and slagging reactions of FeO is summarized as follows. When the simulated cohesive zone is initially formed, the thermal effect is the main cause of the FeO solid-state deformation. Thus, the pores in the packed bed are filled, and the thickness of the cohesive zone shrinks by up to 25 pct at the average rate of approximately 0.20 pct/K. The gaseous reduction of FeO participated by CO further increases the shrinkage by another 25 pct at 1273 K. Then, the slagging reaction of FeO becomes the driving force for the shrinkage at the rate of less than 0.07 pct/K, and the increasing amount of produced metallic iron at the same time retards the shrinkage. By contrast, when the temperature is over 1573 K, the unreacted FeO rapidly softens and then melts, and the SR can increase up to 0.41 pct/K. In addition, when the temperature is over 1623 K, the melting and dripping of metallic iron after carbonization also positively contributes to the fast shrinkage of the thickness of the simulated cohesive zone.

IV. INTERACTION BETWEEN THE REDUCTION AND SLAGGING OF FeO-X BINARY MIXTURE

A. Experimental Schemes and Sample Preparation

Assuming that Fe_2O_3 and Fe_3O_4 in the iron-bearing burden materials are reduced to FeO by the indirect reduction in the upper lump zone, the burden composition in the region above the cohesive zone is calculated

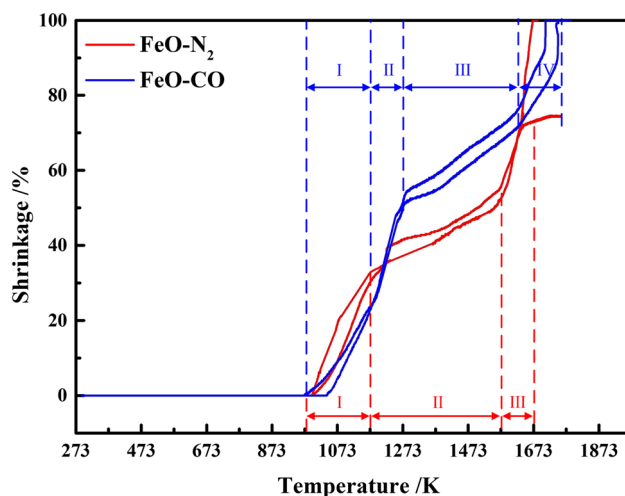


Fig. 10—Comparison of the shrinkages with respect to the temperature between FeO-CO and FeO-N₂ schemes.

based on the mass balance of typical blast furnace raw materials conditions. The results are summarized in Table III. The first experimental group of designed schemes for $\text{FeO}:\text{CaO}:\text{SiO}_2:\text{MgO}:\text{Al}_2\text{O}_3$ is 70:10:10:5:5 pct in mass fraction as shown in Table IV. For FeO-X binary mixture samples, the preparation is almost similar to that for FeO samples, except that the additive oxide powders should be uniformly mixed in advance with the ferrous oxalate powders (Figure 2). The composition of the prepared FeO-X binary samples are measured by XRD (PANalytical B.V. D/max2500/PC Cu K_α), and the results are shown in Figure 11.^[26]

The main composition of the prepared FeO-CaO, FeO-SiO₂, FeO-MgO and FeO-Al₂O₃ binary mixtures are CaO-Fe₃O₄ (melting point, 1377 K), 2FeO-SiO₂ (fayalite, melting point, 1462 K), MgO-FeO (solid solution; melting point, 2064 K), and 2Al₂O₃·FeO (spinel; melting point, 2053 K), respectively, with the remaining

Table III. The Initial Composition of Burden in the Region Above Cohesive Zone Based on Mass Balance Calculation

Composition	FeO	CaO	SiO ₂	MgO	Al ₂ O ₃
Mass kg/tHM	1208.92	160.31	144.46	41.36	60.74
Mass fraction pct	74.79	9.93	8.94	2.58	3.76

Table IV. The First Experimental Group of Designed Schemes for FeO-X Binary Mixture (Unit: g)

Schemes	FeO	CaO	SiO ₂	MgO	Al ₂ O ₃
1-FeO-CaO-CO	87.50	12.50	—	—	—
1-FeO-SiO ₂ -CO	87.50	—	12.50	—	—
1-FeO-MgO-CO	93.33	—	—	6.67	—
1-FeO-Al ₂ O ₃ -CO	93.33	—	—	—	6.67

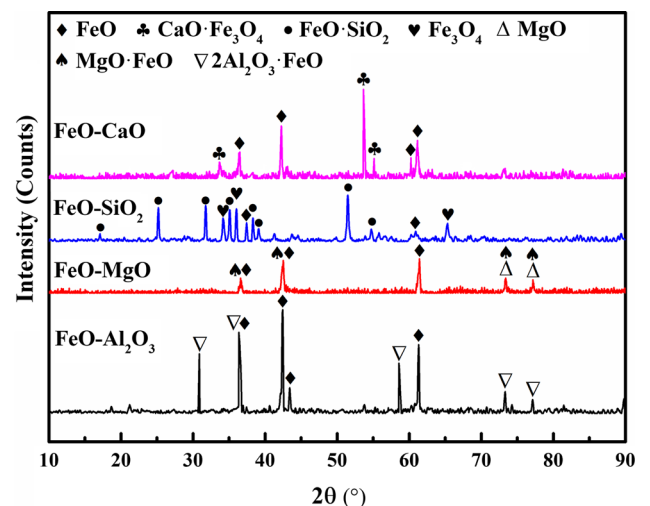


Fig. 11—XRD results of the prepared FeO-X binary mixture samples before the softening–melting experiment.

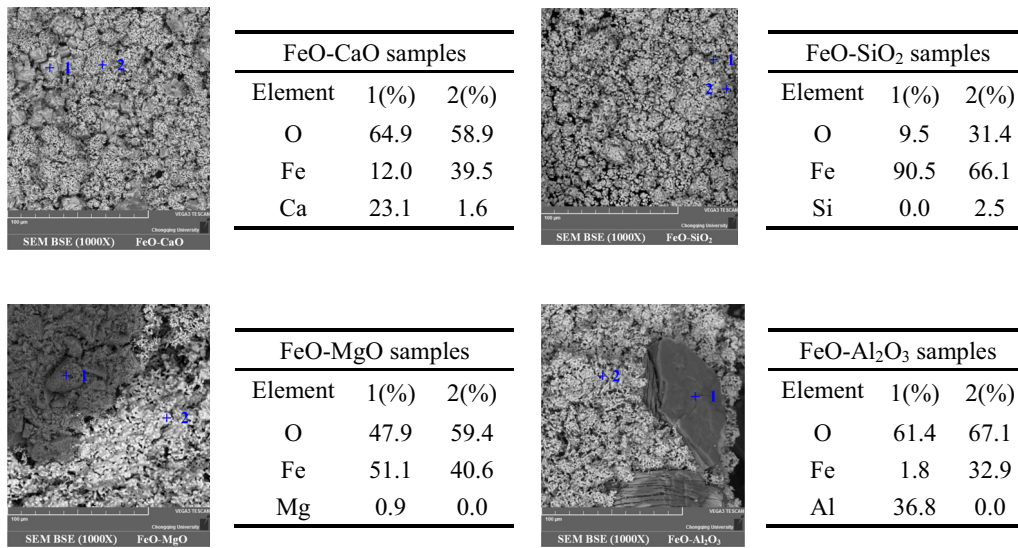


Fig. 12—Microstructures of the prepared FeO-X binary mixture samples before the softening–melting experiment.

unreacted FeO or other oxides. Furthermore, the microstructures based on SEM-EDS (VEGA3 TES-CAN) analysis are compared in Figure 12.

CaO or its compound particles, that have a cubic shape with sharp edges and particle size of less than 20 μm , are dispersedly distributed in the FeO particles. Moreover, Al₂O₃ or its compound particles with length of 100 μm and width of less than 50 μm are dispersedly distributed in the FeO particles. By contrast, the fayalite phase and MgO·FeO solid solution are not obviously found in the prepared binary mixture samples.

B. Results and Discussion

The prepared FeO-X binary mixture samples are used for the subsequent softening–melting experiments. The curves of the shrinkage with respect to the temperature are drawn and divided into individual stages in Figure 13, and the calculated SRs are listed in Table V.

In the first stage, the individual FeO-X binary mixture samples are heated to 1173 K under N₂ atmosphere. Given the relatively low concentrations of SiO₂ and Al₂O₃ in the mixture, their shrinkages are primarily affected by FeO and start as early as 973 K. By contrast, the forming fayalite and spinel restrain the SRs below 0.16 pct/K. MgO exists in the FeO·MgO solid solution. Although the shrinkage start temperature is delayed to approximately 1073 K, its SR is maintained at 0.22 pct/K. By contrast, CaO·Fe₃O₄ greatly increases the SR to 0.42 pct/K, nearly twice as fast as the other results, and the shrinkage at 1173 K exceeds 50 pct.

When CO is introduced in the second stage, all SRs of the FeO-X binary mixtures are slower than the counterpart in the base case (0.31 pct/K). This result indicates that the slagging reaction dominates the shrinkage in this stage regardless of the effects of the added compounds on the reduction.

In the following third or/and fourth stages, different schemes demonstrate the diverse behaviors. Given the fastest SRs in the former two stages, the shrinkage in the FeO-CaO scheme is above 70 pct at 1273 K. Further increase in temperature only facilitates the melting of the unreacted CaO·Fe₃O₄ and FeO, and the related SR is below 0.030 pct. Meanwhile, the poor permeability of the packed bed probably presents an obstacle for the carbonization and dripping of reduced metallic iron. Thus, the final shrinkage of the packed bed stops at 86 pct. Given that only a limited proportion of FeO in FeO·MgO solid solution is free to participate the reduction reaction and no dripping of metallic iron is detected, the SR, which is dominated by the slagging reaction of FeO, is 0.069 pct/K. For FeO-SiO₂, the increasing temperature gradually promotes the reduction of fayalite, resulting in relatively fast SR (0.076 pct/K) compared with the base case. When the temperature exceeds 1512 K in the fourth stage, the unreduced fayalite melts and drips to shrink at a low rate of 0.017 pct/K. For FeO-Al₂O₃, the spinel with extremely high melting temperature is present in the melting phase as the solid-phase particles. Thus, the SRs decrease to 0.045 and 0.10 pct/K in the third and fourth stages, respectively.

CaO notably hastens the shrinkage of FeO, especially before 1273 K, and the final shrinkage stops at 86 pct. The formation of the solid solution FeO·MgO not only postpones the shrinkage start temperature but also suppresses the shrinkage controlled by the reduction in the second stage. Despite the low concentration of Al₂O₃, the formed spinel with high melting temperature acts as the solid-phase particles and generally decreases the SRs of the whole stages. The fayalite decreases the SRs at low temperature but subsequently increases the SR because of the gradually improving reducibility, which restrains the further melting and dripping of fayalite.

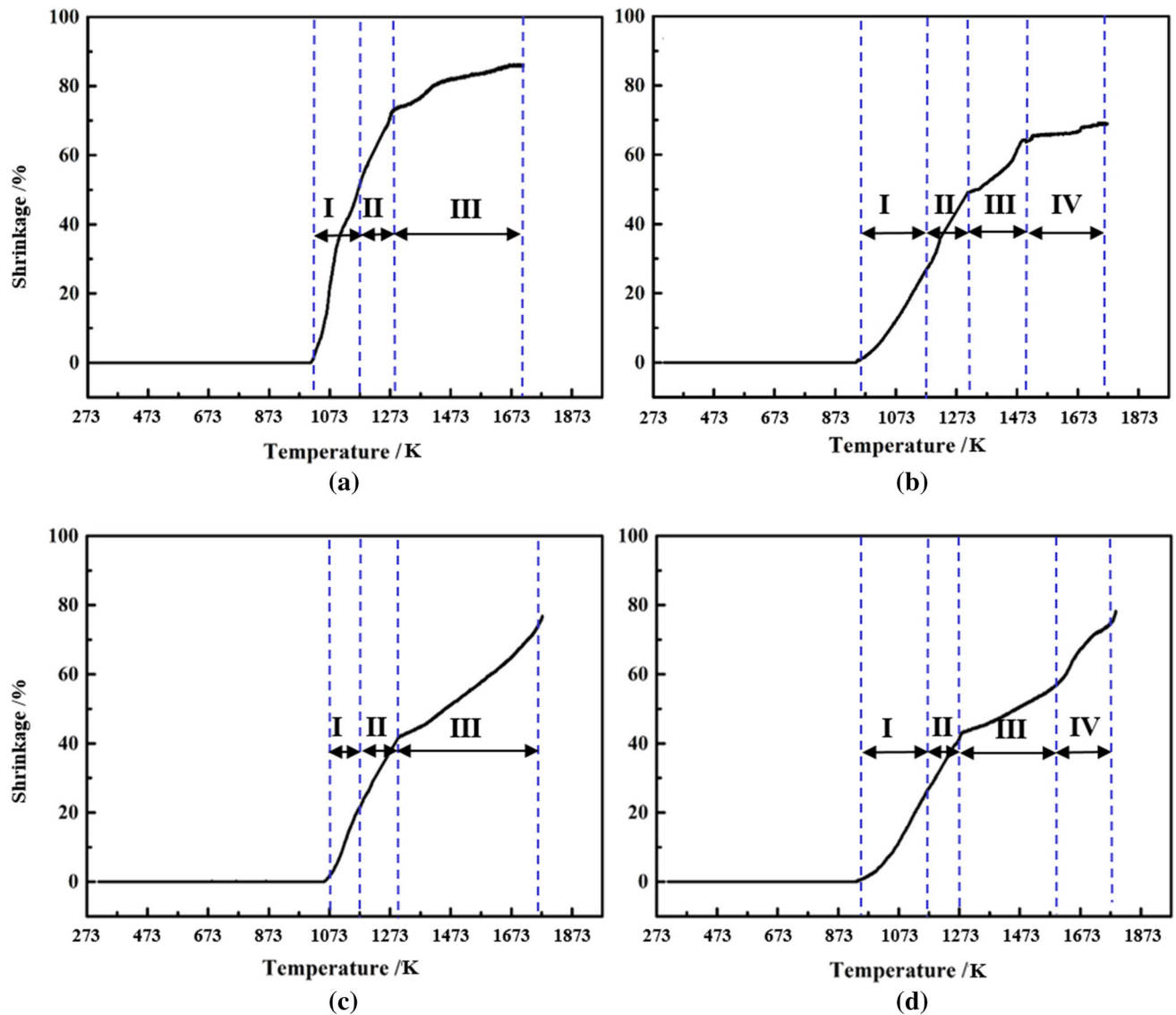


Fig. 13—The curves of shrinkage with respect to the temperature and corresponding stages division (a) 1-FeO-CaO-CO, (b) 1-FeO-SiO₂-CO, (c) 1-FeO-MgO-CO, and (d) 1-FeO-Al₂O₃-CO.

Table V. The SRs of Different Stages in 1-FeO-X-CO Schemes (Unit: Pct/K)

Schemes	First Stage	Second Stage	Third Stage	Fourth Stage
FeO-CO	0.17	0.31	0.067	0.18
1-FeO-CaO-CO	0.42	0.19	0.029	n/a
1-FeO-SiO ₂ -CO	0.14	0.15	0.076	0.017
1-FeO-MgO-CO	0.22	0.16	0.069	n/a
1-FeO-Al ₂ O ₃ -CO	0.16	0.15	0.045	0.10

C. Interaction Between Reduction and Slagging Reactions

To further elucidate the interaction between reduction and slagging reactions, the mass fraction of X in FeO-X binary mixture is doubled to FeO:CaO:SiO₂:MgO:Al₂O₃ = 40:20:20:10:10 pct in mass fraction. Pure N₂

is also introduced for comparison. Thus, the second experimental group of designed schemes for FeO-X binary mixture is clarified in Table VI. The shrinkages under the different conditions vary with the temperature. The corresponding results are compared in Figure 14, and the calculated SRs are collected in Table VII.

Table VI. The Second Experimental Group of Designed Schemes for FeO-X Binary Mixture (Unit: g)

Schemes	FeO	CaO	SiO ₂	MgO	Al ₂ O ₃
2-FeO-CaO-CO	66.67	33.33	—	—	—
2-FeO-CaO-N ₂	66.67	33.33	—	—	—
2-FeO-SiO ₂ -CO	66.67	—	33.33	—	—
2-FeO-SiO ₂ -N ₂	66.67	—	33.33	—	—
2-FeO-MgO-CO	80.00	—	—	20.00	—
2-FeO-MgO-N ₂	80.00	—	—	20.00	—
2-FeO-Al ₂ O ₃ -CO	80.00	—	—	—	20.00
2-FeO-Al ₂ O ₃ -N ₂	80.00	—	—	—	20.00

When the concentration of CaO further increases, the unslugged CaO in the binary mixture resists to shrink. Thus, the SR decreases to 0.16 pct/K before 1173 K and to 0.015 pct/K at higher temperature without reduction participation. After CO is introduced in the second

stage, although the SR temporally increases to 0.30 pct/K, it quickly drops to 0.021 pct/K after 1273 K. Hence, the eventual shrinkage is 72.5 pct, which is less than its counterpart in 1-FeO-CaO-CO scheme by approximately 13 pct. In addition, the shrinkage of the samples under N₂ atmosphere was finally approximately 40 pct, which indicates that the produced CaO·Fe₃O₄, even with low melting temperature, does not drip easily after melting.

By contrast, when SiO₂ is added, the fayalite not only has a low melting temperature but also tends to drip once the temperature exceeds 1436 K in 2-FeO-SiO₂-N₂. Moreover, the SR below 1173 K will become faster as more fayalite is produced. The poor reducibility of fayalite under high proportion of SiO₂ in the mixture restrains the SR in the second stage to 0.16 pct/K, but it gradually improves with the increasing temperature.

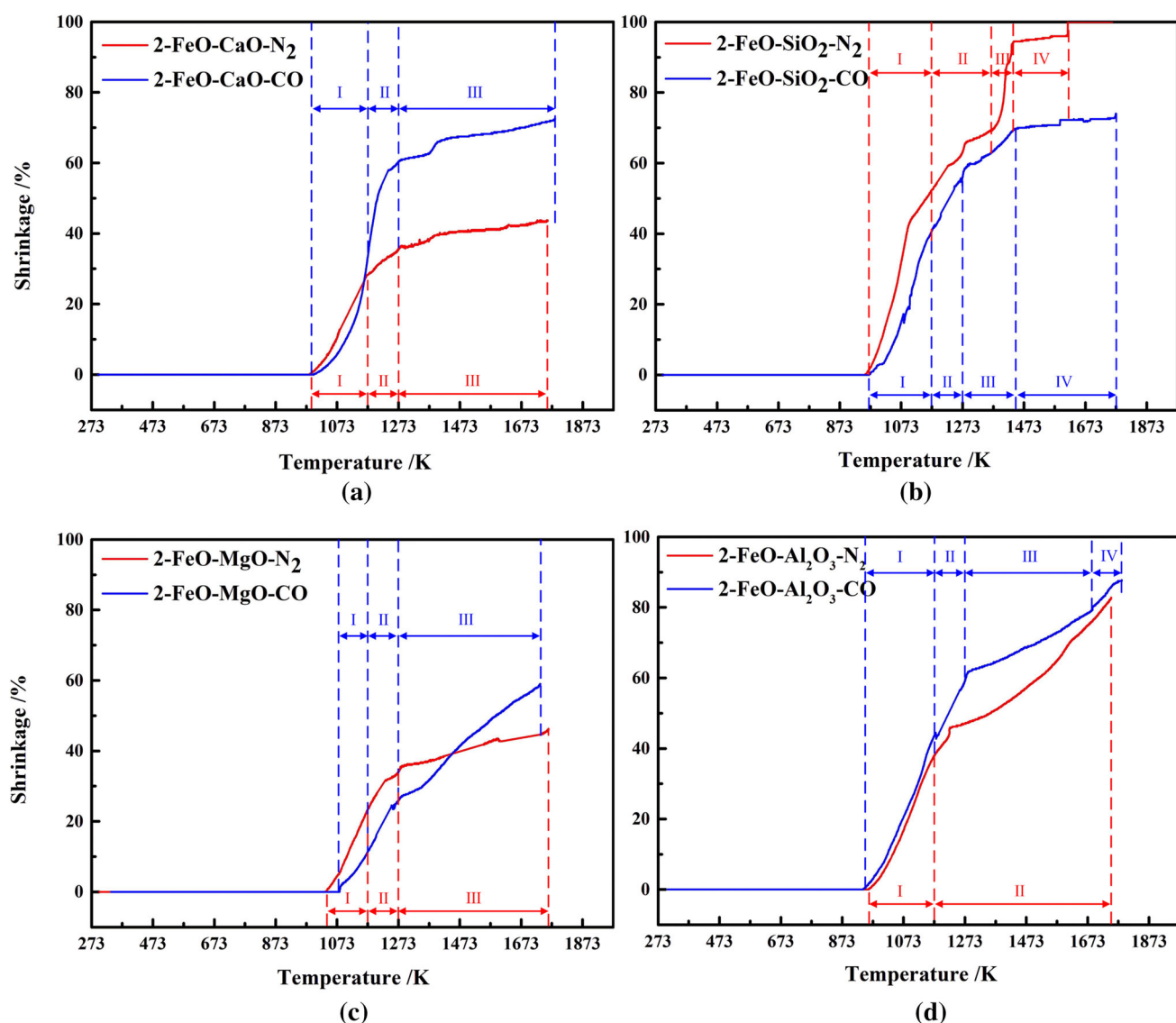


Fig. 14—The curves of shrinkage with respect to the temperature and corresponding stages division (a) 2-FeO-CaO-CO/N₂, (b) 2-FeO-SiO₂-CO/N₂, (c) 2-FeO-MgO-CO/N₂, and (d) 2-FeO-Al₂O₃-CO/N₂.

Table VII. The SRs of Different Stages in 2-FeO-X-CO/N₂ Schemes (Unit: Pct/K)

Schemes	First Stage	Second Stage	Third Stage	Fourth Stage
FeO-CO	0.17	0.31	0.067	0.18
FeO-N ₂	0.20	0.043	0.41	—
2-FeO-CaO-CO	0.16	0.30	0.021	—
2-FeO-CaO-N ₂	0.16	0.069	0.015	—
2-FeO-SiO ₂ -CO	0.27	0.16	0.077	0.009
2-FeO-SiO ₂ -N ₂	0.33	0.098	0.49	0.027
2-FeO-MgO-CO	0.13	0.15	0.072	—
2-FeO-MgO-N ₂	0.18	0.10	0.023	—
2-FeO-Al ₂ O ₃ -CO	0.21	0.18	0.044	0.098
2-FeO-Al ₂ O ₃ -N ₂	0.19	0.072	—	—

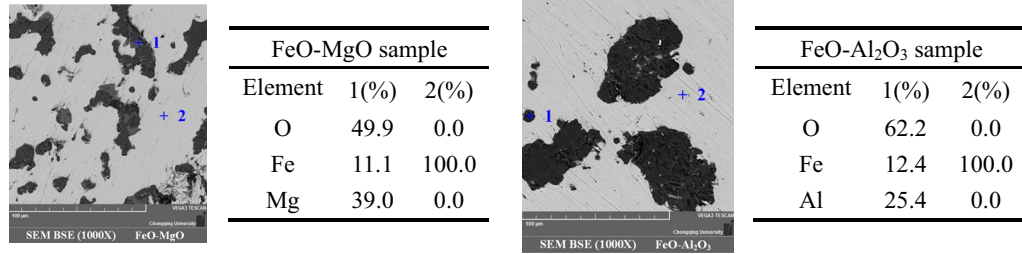


Fig. 15—Microstructures of FeO-MgO and FeO-Al₂O₃ binary mixture samples after the softening–melting experiment.

Further increase in the MgO concentration in the FeO-MgO solid solution forms a skeletal-like structure. The microstructure of the samples after the softening–melting experiment is analyzed using SEM-EDS, and the results are shown in Figure 15. MgO or the solid solution forms small or long and narrow phases, and most of particles have a size of less than 20 μm and almost uniformly distributed in the iron-based matrix. Thus, they play as a “skeletal” structure to resist the shrinkage. The more MgO is added to the solid solution, the stronger is the resistance to deformation. This characteristic decreases the SRs to below 0.18 pct/K before 1173 K. However, the case can be improved when the reduction of FeO by CO begins at higher temperature. However, given that only a limited proportion of FeO in the solid solution can be reduced, the increasing MgO concentration in the mixture has little influence on the reduction reaction. Thus, the SRs in the following stages decrease to as low as 0.023 pct/K.

For FeO-Al₂O₃, the microstructure of the samples after the softening–melting experiment is also shown in Figure 15. The FeO·Al₂O₃ spinel forms large and wide phases, and its average size reaches above 60 μm. The dispersed distribution of FeO·Al₂O₃ spinel has less impact than the FeO-MgO solid solution on the shrinkage behavior at low temperature. Further reduction of the unslagged FeO helps maintain the SR in the second stage at 0.18 pct/K. However, the slowest reduction rate reduces the SR in the following stage to approximately 0.044 pct/K. When the temperature is over 1673 K, the residual FeO melts and increases the SR to approximately 0.098 pct/K. The results are summarized in Figure 16.

V. CONCLUSIONS

A new index SR is established to investigate the transient interaction between reduction and slagging reactions of FeO in the simulated cohesive zone of the blast furnace. The index is based on the shrinkage of the thickness of FeO or FeO-X binary mixture sample packed bed with respect to temperature in the softening–melting experiment. The shrinkage of FeO or FeO-X binary mixture samples are primarily attributed to the gaseous reduction participated by CO, the slagging reaction caused by thermal effect, or even both reactions.

At low temperature (below 1173 K), FeO is slagging on its own by deformation. The pores in the packed bed are filled when the bed shrinks at approximately 0.20 pct/K. The addition of CaO or SiO₂ under the proper proportion can increase the SR up 0.42 pct/K, whereas MgO decreases the SR to as low as 0.13 pct/K by forming a solid–solution phase. By contrast, the effect of Al₂O₃ can be negligible under the present experimental conditions.

Once CO is introduced, the packed bed shrinkage generally accelerates, which indicates that reduction, instead of the slagging reaction, dominates the shrinkage between 1173 K and 1273 K. Thereafter, the SRs drops to 0.021, 0.077, 0.072, and 0.044 pct/K with reduction participation and changes to 0.015, 0.49, 0.023, and 0.072 pct/K without reduction participation for FeO-CaO, FeO-SiO₂, FeO-MgO, and FeO-Al₂O₃ binary mixtures, respectively. Thus, the further shrinkage with the increasing temperature is mainly controlled by the slagging reaction when CaO is added, by the reduction

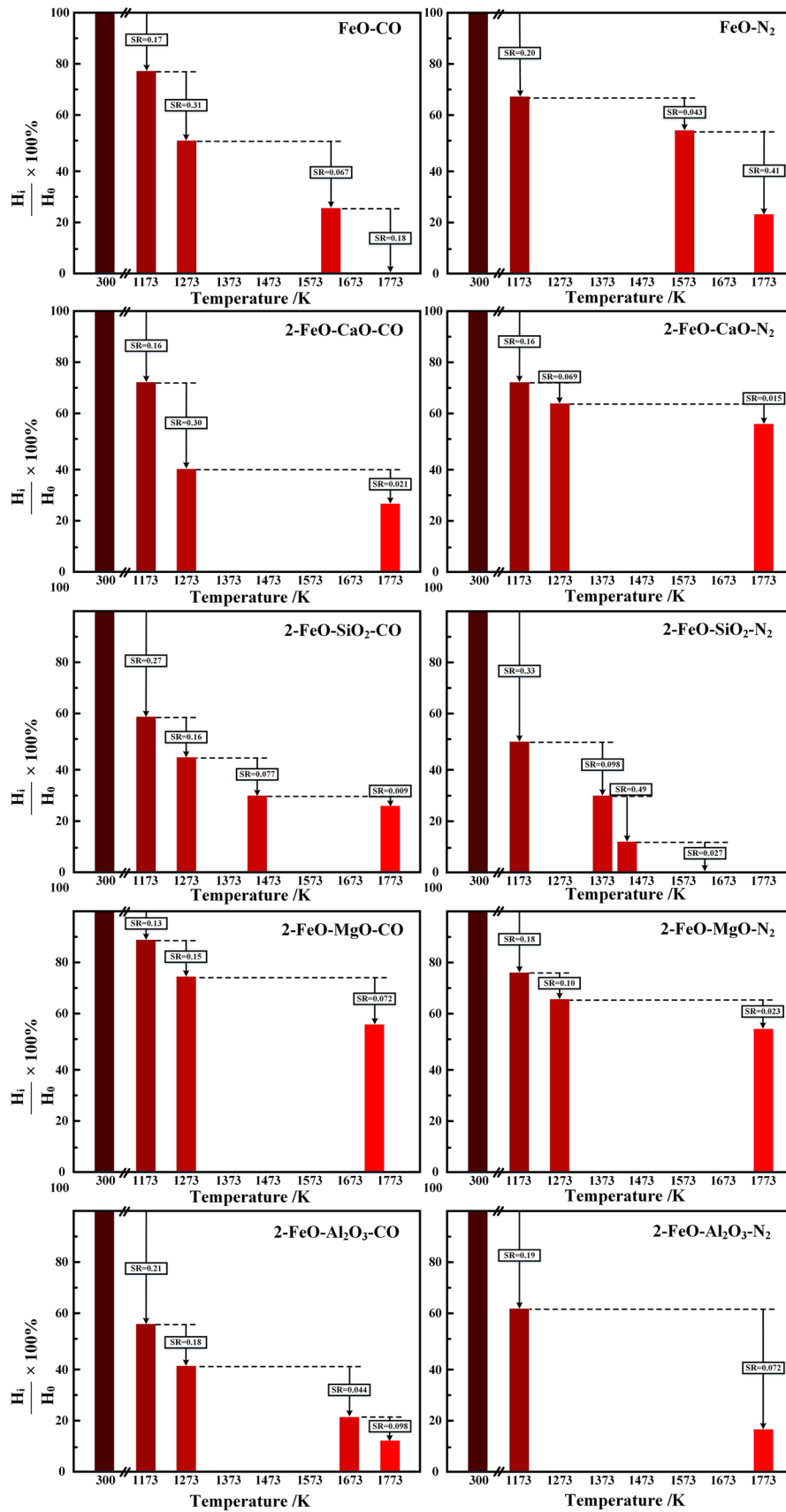


Fig. 16—Summary of the interaction between reduction and slugging reactions of FeO and FeO-X binary mixture in the form of SR.

reaction when SiO₂ or Al₂O₃ is added, or by both reactions when MgO is added.

ACKNOWLEDGMENTS

The authors appreciate the valuable suggestions and comments from the anonymous reviewers, key readers and editors. The authors are also grateful to the National Natural Science Foundation of China (51304257, 91634106) for their support extended to this project, and the Natural Science Foundation of Chongqing, China (cstc2015jcyjA50014), and the financial support from the National Natural Science Foundation of China (51374263, 51474042) is also gratefully acknowledged.

REFERENCES

1. N.J. Busby, T.A.T. Fray, and D.C. Goldring: *Ironmak Steelmak.*, 1994, vol. 21, pp. 229–36.
2. U. Leimalm, S. Forsmo, A. Dahlstedt, O.L. Sundqvist, and B. Bjorkman: *Trans Iron Steel Inst Jpn.*, 2010, vol. 50, pp. 1396–1405.
3. K. Ono, K. Yamaguchi, A. Shigemi, N. Nishida, and K. Kanbara: *Tetsu-to-Hagané*, 1980, vol. 65, pp. 505–14.
4. M. Hino and T. Nagasaka: *Metall. Mater. Trans. B*, 1999, vol. 30B, pp. 671–83.
5. K.F. Zhang, S.L. Wu, W. Huang, X.L. Liu, J. Zhu, and K.P. Du: *6th International Symposium on High-Temperature Metallurgical Processing*. Springer, Berlin, 2015, pp. 155–61.
6. I. Shigaki, M. Sawada, M. Maekawa, and K. Narita: *ISIJ Int.*, 2010, vol. 21, pp. 862–69.
7. X. Jiang, G.S. Wu, M.F. Jin, and F.M. Shen: *J. Northeast. Univ.*, 2006, vol. 27, pp. 1358–61.
8. S. Ueda, T. Kon, T. Miki, S.J. Kim, and H. Nogami: *Metall. Mater. Trans. B*, 2016, vol. 47B, pp. 2371–77.
9. J. Szekely and Y. El-Tawil: *Metall. Trans. B*, 1976, vol. 7, pp. 490–92.
10. N. Towhidi and J. Szekely: *Metall. Trans. B*, 1983, vol. 14, pp. 359–67.
11. D.D. Wang, J. Xu, K.H. Ma, Y. Xu, J. Dang, M.Y. Kou, X.W. Lv, and L.Y. Wen, *Int. J. Hydrog. Energy*, 2017.
12. K.M. Hutchings, J.D. Smith, S. Yoruk, and R.J. Hawkins: *Ironmak. Steelmak.*, 1987, vol. 14, pp. 103–09.
13. R. Corbari and R.J. Fruehan: *Metall. Mater. Trans. B*, 2010, vol. 41B, pp. 318–29.
14. E.J. Worrall and K.S. Coley: *Metall. Mater. Trans. B*, 2010, vol. 41B, pp. 813–23.
15. E.T. Turkdogan and J.V. Vinters: *Metall. Mater. Trans. B*, 1972, vol. 3B, pp. 1561–74.
16. J. Szekely and C. Karatas: *Metall. Trans. B*, 1978, vol. 9B, pp. 147–50.
17. A.A. El-Geassy: *Trans. Iron Steel Inst. Jpn.*, 2006, vol. 25, pp. 449–58.
18. H.T. Wang and H.Y. Sohn: *Trans. Iron Steel Inst. Jpn.*, 2015, vol. 55, pp. 706–08.
19. H. Inoue, Y. Kiritani, and Y. Takahashi: *Bull. Res. Inst. Miner. Dress. Metall. Tohoku Univ.*, 1976, vol. 31, pp. 127–36.
20. M. Moukassi, M. Gougeon, P. Steinmetz, B. Dupre, and C. Gleitzer: *Metall. Trans. B*, 1984, vol. 15B, pp. 383–91.
21. N. Shigematsu and H. Iwai: *Trans. Iron Steel Inst. Jpn.*, 2006, vol. 28, pp. 206–13.
22. S. Hayashi and Y. Iguchi: *ISIJ Int.*, 1992, vol. 36, pp. 1000–08.
23. T. Nishimura, K. Higuchi, M. Naito, and K. Kunitomo: *ISIJ Int.*, 2011, vol. 51, pp. 1316–21.
24. M. Matsumura, M. Hoshi, and Takazo. Kawaguchi: *Trans. Iron Steel Inst. Jpn.*, 2005, vol. 45, pp. 594–602.
25. Y. Hosotani, K. Yamaguchi, T. Orimoto, K. Higuchi, T. Kawaguchi, and H. Goto: *Tetsu-to-Hagané*, 2009, vol. 83, pp. 97–102.
26. D.D. Wang, K.H. Ma, Y. Xu, J. Xu, and L.Y. Wen: in *Applications of Process Engineering Principles in Materials Processing, Energy and Environmental Technologies*, S.J. Wang, M. Free, S. Alam, M.M. Zhang, and P.R. Taylor, eds., Springer, San Diego, 2017, 1st Ed., pp. 251–58.